Nuclear Engineering and Technology 52 (2020) 1579–1586

Contents lists available at ScienceDirect

Nuclear Engineering and Technology

journal homepage: www.elsevier.com/locate/net

Original Article

Effect of dissimilar metal SENB specimen width and crack length on stress intensity factor

A. Ramachandra Murthy*, M. Muthu Kumaran, M. Saravanan, P. Gandhi

CSIR-Structural Engineering Research Centre, Taramani, Chennai, 600113, India

ARTICLE INFO

Article history:
Received 4 October 2019
Received in revised form
4 December 2019
Accepted 16 December 2019
Available online 19 December 2019

Keywords:
Dissimilar metal joint
Finite element analysis
Dissimilar metal single edged notch bending specimen
Constraint effect
LEFM

ABSTRACT

Dissimilar metal joints (DMJs) are more common in the application of piping system of many industries. A 2- D and 3-D finite element analysis (FEA) is carried out on dissimilar metal Single Edged Notch Bending (DMSENB) specimens fabricated from ferritic steel, austenitic steel and Inconel − 182 alloy to study the behavior of DMJs with constraints by using linear elastic fracture mechanics (LEFM) principles. Studies on DMSENB specimens are conducted with respect to (i) dissimilar metal joint width (DMJW) (geometrical constraints) (5 mm, 10 mm, 20 mm, 30 mm and 50 mm) (ii) strength mismatch (material constraints) and (iii) crack lengths (16 mm, 20 mm and 24 mm) to study the DMJ behavior. From the FEA investigation, it is observed that (i) SIF increases with increase of crack length and DMJWs (ii) significant constraint effect (geometry, crack tip and strength mismatch) is observed for DMJWs of 5 mm and 10 mm (iii) stress distribution at the interfaces of DMSENB specimen exhibits clear indication of strength mismatch (iv) 3-D FEA yields realistic behavior (v) constraint effect is found to be significant if DMJW is less than 20 mm and the ratio of specimen length to the DMJW is greater than 7.4.

1. Introduction

The application of dissimilar metal joints in the coolant system of aerospace, marine (ship building), nuclear, bio medical is vital due to its prominence of mechanical and thermal properties. In the case of long distance pipelines, dissimilar metal joints (DMJs) are inevitable for the use of petroleum transport and natural gas around the world [1]. Also, DMJs are used in the nuclear, oil refineries and chemical industries [2]. Joints are vulnerable locations [3] since they are prone to different types of flaws. Life prediction of highly ductile and dissimilar metal components using fracture analysis is paramount in engineering applications for structural integrity assessments [4]. The structural integrity assessment and life evaluation is mainly influenced by DMJs due to its constraints in material, geometry and loading. Primary pipes in nuclear power plants caused leak of radioactive into water due to the through wall crack in the DMJs [5]. Understanding of DMJs is highly complex due to its heterogeneity in microstructure, mechanical, thermal, fracture properties and geometry. Wang et al. [6] reported that, DMJs are highly heterogeneous due to its microstructure, mechanical and fracture properties. The distribution of mechanical properties fluctuates drastically in DMJs due to its complex microstructure localization which leads to inhomogeneous [5]. Material mismatch constraint arises in the DMJs due to the heterogeneity [7,8]. Material mismatch was influenced by the crack driving force in DMJs under service condition [9]. Analytical or experimental fracture investigation on DMJs is highly complex due to the microstructure, mechanical, thermal and fracture properties [3,10].

Safety assessment of real structures with complex crack configurations was carried out by Bakker [11] on Single Edge Notched Bending (SENB) specimen using 2-D and 3-D Finite Element Analysis (FEA). Xu et al. [12] conducted 2-D FEA with geometric constraints to predict the crack growth behavior of SENB specimen (thin walled pipeline steels) and was characterized using experimentation. Ductile crack growth behavior of dissimilar metal SENB (DMSENB) specimen were studied by Wang et al. [6], using 2-D FEA. Samal et al. [2], investigated DMSENB specimen using FEA to understand the fracture behavior using experimental validation and was in satisfactory manner. Yang et al. [13], experimented SENB specimen to evaluate the crack resistance curve for the low alloy carbon steel (Ferritic steel) wherein 2-D and 3-D FEAs were conducted under in-plane and out-of-plane constraints. Experimentation of DMSENB specimen used in nuclear plants was carried out by Wang et al. [3], to

* Corresponding author.
E-mail addresses: murthyarc@serc.res.in (A.R. Murthy), kumaranmahan@gmail.com (M. Muthu Kumaran), sardirajm@serc.res.in (M. Saravanan), pgandhi@serc.res.in (P. Gandhi).

https://doi.org/10.1016/j.net.2019.12.018

understand the local fracture resistance, crack growth behavior and integrity assessment. Wang et al. [14], investigated the SENB specimen of low alloy steel using FEA based on the load-independent as constraint parameter. Local fracture resistance of induced crack depth was evaluated by Yang et al. [15], using experimentations on SENB specimen under in-plane constraint for several crack depths. Unified correlation of in-plane and out-of-plane constraints was used by Yang et al. [16], to establish the fracture resistance of DMSENB specimen subjected to quasi static loading with different crack depths (in-plane constraint) and specimen thickness (out-of-plane) using both experimentation and 3-D FEA. Kumar et al. [4], conducted FEA on DMSENB specimen using eXtended Finite Element Method (XFEM) to study the stable crack under plane stress condition with strain field discontinuities due to the material discontinuity. Microscopic analysis of DMSENB specimen was experimented by Della Rovere et al. [17], to study the local fracture resistance using scanning electron microscopy. Gonzalez et al. [18], studied the SENB specimen (visco-elastic material) using boundary element method to compute the SIF based on linear Elastic Fracture Mechanics (LEFM) approach. Both the experimentation and 3-D FEA of SENB specimen were carried out by Mu et al. [19], to evaluate the in-plane and out-of plane constraints. Fracture resistance of DMJs at interface regions in SENB specimen was investigated systematically by Fan et al. [9], using 2-D FEA. Fan et al. [20], investigated the local failure behavior of DMJ interfaces in the DMSENB specimen using FEA to understand the mechanical heterogeneity, crack growth path, and fracture resistance; and reported that the evaluation of fracture resistance with respect to the crack locations could be done based on the reliable structural assessments and failure analyses in accurate manner wherein the numerically predicted crack path found to be similar with experimental studies. Fracture behavior of coolant system in nuclear power plants was assessed by Kim et al. [21], using crack growth resistance curve with respect to the loading rate. Musraty et al. [22], conducted FEA to study the fracture mechanism of pipe ring noched bend (PRNB) and SENB specimen. Predicted crack growth resistance curves from the numerical analysis were considered by Younise et al. [7], to understand the material heterogeneity effect of DMSENB specimen using micromechanical experimentations. Experimental investigation of DMSENB specimen under quasi-static loading was carried out by Yang et al. [23], to understand the fracture mechanism under the interaction effect of in-plane and out-of-plane constraints and is found to be ductile (high), local brittle, mixed and local ductile fracture mechanisms for low out-of-plane and in-plane constraint, low in-plane and high out-of-plane constraint, high in-plane and low out-of-plane constraints and high in-plane and high out-of-plane constraints respectively. Experimental investigation were carried out by Tang et al. [24], on DMJs of DMSENB specimen at different regions using normalization and unloading compliance method; and the initiation of fracture toughness was found to be similar in both methods. Dai et al. [25], investigated the DMJs of SENB specimen to study the ductile behavior under different material constraints using 3-D FEA. Microstructural studies on DMJs were carried out by Karthick et al. [8], to investigate the material mismatch effect. SENB (carbon/glass/PolyEther ether ketone (PEEK) thermoplastic hybrid laminated composites) specimen under thermo mechanical loading using LEFM principles were investigated by Vieille et al. [26], in addition to experimentation and 2-D digital image correlation (DIC). Ductile crack growth behavior of X80 pipeline steel DMJs were evaluated by Qiang et al. [1], using both experiments and FEA. Zuo et al. [27], studied fracture behavior of Meso-SENB with oblique discontinuities using 2-D FEA to evaluate the SIF.

SIF is a vital parameter to understand the assessment of structural integrity of the components/structures. Accurate assessment of structural integrity is based on the relation between the specimens and structures; and is an important issue [13]. Local fracture behavior and structural integrity assessment were studied by Wang et al. [5], based on the mechanical properties. An accurate assessment of the structural integrity of DMJs based on sound fracture principles is quite complex and is unavailable [6,23]. Constraining effect influences the structural integrity based on the fracture mechanics in order to improve the fracture assessments [19]. Structural integrity assessment and failure analysis were studied by Fan et al. [20], on DMJs. Currently, fitness-for-service (FFS) assessment derived from the engineering critical assessment (ECA) methodology is purely based on the assumption of material homogeneity [9]. Fracture toughness of the material is influenced by thickness [28]. Consideration of the thickness effects (Out-of-plane) in the analysis represents the cracked bodies in real world. 2-D analysis will provide conservative results and it takes lesser computational effort compared to 3-D. But, 3-D analysis is very much essential to know the behavior of the component across the thickness. The analysis will be decided based on the type and nature of the problem. For structural integrity, the analysis of 3-D cracked bodies is very much essential to understand the fracture behavior. Constraint plays a major role in studying the behavior of fracture (Material fracture toughness) [13]. In-plane constraint increases with out-of-plane constraint effect [19]. Constraint conditions and stress around the crack tip are the derivatives of the strength mismatch to understand the fracture mechanism and crack growth path [15]. The study of crack tip constraint was used to understand the transferability of fracture toughness which could be applicable to the geometrical change [12].

Fracture studies on DMJs behavior are very limited due to the complexities [2]. The analysis of crack growth behavior on DMJs is very limited [6]. Very limited studies have been carried out on constraint effect to understand the fracture behavior of the DMJs [23]. Ductile fracture can be characterized by using LEFM or EPFM (Elastic-Plastic Fracture Mechanics) principles [7]. Wang et al. [29], used srawley equation [30] to evaluate SIF. Implementation of XFEM can be useful to handle the mesh refinement issues around the crack tip. In XFEM, there is no necessity of mesh refinements around the crack tip. Thickness effect influences the SIF due to stress state in 3-D. Very limited studies were carried out on DMSENB specimen using 3-D FEA in LEFM approach wherein the predicted crack growth is not carried out [1–3,6,9,10,13–16,20,23,25]. To the best of author's knowledge, detailed studies on fracture using FEAs on DMSENB with the support of available analytical solutions in 2-D (contour integral method) and 3-D (XFEM) based on the LEFM principles have not been carried out. Hence an attempt is made in this present work to overcome the limitations aforementioned.

2. Background theory for the numerical investigation

XFEM has numerous advantages like significant improvement in convergence, accuracy, discontinuity and mesh independencies. The contour integral method and eXtended Finite Element Method (XFEM) are used to evaluate the SIF for 2-D and 3-D respectively. The following section briefly discusses the methodology.

2.1. Contour integral method formulation

The crack propagation can be predicted by using the contour integral by assigning the crack front, crack tip and crack direction. The domain integral method [31] is used to compute the SIFs and continue by tracing the predicted crack path with its size. Fracture parameters such as J-integral, SIF etc., can be extracted with better accuracy even in the presence of coarser FE mesh contours surrounding the crack tip. These contour integrals are evaluated by the

domain integral method. SIF is related to the energy release in the linear elastic analysis and vice versa. In this method, the line integral is used to evaluate the predicted crack growth enclosing the domain based on the maximum tangential stress as crack initiation criterion. Contour domain is represented as shown in Fig. 1 [32],

$$J = \oint_{\Gamma} \left(\sigma_{ij} \frac{\partial u_i}{\partial x_1} - W\delta_{1j} \right) \frac{\partial q_1}{\partial x_j} dA \tag{1}$$

Where σ_{ij} = Cauchy stress tensor; u = displacement vector; W = strain energy density; δ_{1j} = Kronecker delta; q_1 = non zero weighing function based on the domain enclosure and A = area enclosed by the closed contour C.

FE formulation in isoparametric space as, 3 × 3 Gaussian quadrature appropriate to the 9-node biquadratic Lagrange element is,

$$J = \sum_{\substack{all\ elements \\ in\ A}} \sum_{p=1}^{9} \left\{ \left[\sigma_{ij} \frac{\partial u_i}{\partial x_1} - W\delta_{1j} \right] \frac{\partial q_1}{\partial x_j} \det\left(\frac{\partial x_k}{\partial \eta_k} \right) \right\}_p w_p \tag{2}$$

Whereas, q_1 and its spatial derivatives can be computed at nine quadrature points and weighted by w_p and determinant of Jacobian matrix, $\det\left(\frac{\partial x_k}{\partial \eta_k}\right)$.

Isoparametric formulation values of q_1 and its spatial derivatives at the quadrature points are computed by,

$$q_1 = \sum_{I=1}^{9} N_I Q_{1I} \tag{3}$$

$$\frac{\partial q_1}{\partial x_i} = \sum_{p=1}^{9} \sum_{k=1}^{9} \frac{\partial N_I}{\partial \eta_k} \frac{\partial \eta_k}{\partial x_i} Q_{1I} \tag{4}$$

Where, N_I = biquadratic shape function; Q_{1I} = value of q_1 associated with the I^{th} node and element (assigned in accordance with a smooth function).

The coordinates (x_1, x_2) in the physical space and the displacements (u_1, u_2) are

$$x_i = \sum_{K=1}^{9} N_K X_{iK} \tag{5}$$

$$u_i = \sum_{K=1}^{9} N_K U_{iK} \;\; ; \;\; i = 1,2 \tag{6}$$

Whereas, U_{iK} and X_{iK} are the nodal displacements and nodal coordinates respectively.

2.2. XFEM formulation

The Motion of interfaces was modeled by Osher et al. [33], implementing the numerical aspects through level set method. Stolarska et al. [34], developed an algorithm to model crack growth by coupling the level set method in XFEM. Sukumar et al. [35], implemented XFEM with fast marching method to evaluate the SIF through the proposed numerical technique by modeling planar cracks in 3-D bodies. An assemblage of FEM and Partition of unity provides an exhaustive tool to evaluate the fracture parameters, and it is named as XFEM based on the enrichment function around the crack tip wherein there is no need of remeshing. XFEM follows the level set method to generate the crack in the domain and it enables better accuracy than other procedures. Crack intersection can be done at anywhere in the specimen by using the enrichment function which is independent of the element size. i.e., there is no need of locating the crack at the element edges to open the crack along its nodes and it is the significance of XFEM. Element discretization has no significance when assigning the crack geometry in the numerical modeling.

An extrinsic enrichment can be approximated by the following form [36],

$$u^h(x) = \sum_{I=1}^{n} N_I(x) \left(u_I + \sum_{j=1}^{n_E(I)} a_{jI} \gamma_j(r,\theta) \right) \tag{7}$$

$$v^h(x) = \sum_{I=1}^{n} N_I(x) \left(v_I + \sum_{j=1}^{n_E(I)} b_{jI} \gamma_j(r,\theta) \right) \tag{8}$$

Where, r and θ are the polar coordinates with origin at the crack tip; $N_I(x)$ = Standard finite elements shape functions; a_{jI} and b_{jI} = enrichment coefficients associated with nodes; $n_E(I)$ = number of coefficients for node I; $n_E(I) = 4$ for this case at the enriched nodes.

The displacement field functions,

$$\{\gamma_I(r,\theta)\}_{i=1}^{4} = \left\{ \sqrt{r}\cos\left(\frac{\theta}{2}\right), \sqrt{r}\sin\left(\frac{\theta}{2}\right), \sqrt{r}\sin\left(\frac{\theta}{2}\right)\sin(\theta), \sqrt{r}\cos\left(\frac{\theta}{2}\right)\sin(\theta) \right\} \tag{9}$$

Combination of Mode I and Mode II loading on near tip displacements fields are,

$$u(x,y) = \frac{K_I}{2\mu}\sqrt{r/2\mu}\cos(\theta/2)\left[k - 1 + 2\sin^2(\theta/2)\right] + \frac{K_{II}}{2\mu}\sqrt{r/2\mu}\sin(\theta/2)\left[k + 1 + 2\cos^2(\theta/2)\right] \tag{10}$$

$$v(x,y) = \frac{K_I}{2\mu}\sqrt{r/2\mu}\sin(\theta/2)\left[k + 1 - 2\cos^2(\theta/2)\right] - \frac{K_{II}}{2\mu}\sqrt{r/2\mu}\cos(\theta/2)\left[k - 1 - 2\sin^2(\theta/2)\right] \tag{11}$$

Where, k = Kolosov constant; K = Stress intensity factor; μ = Poisson's ratio.

2.3. Analytical solution for homogeneous three point SENB specimen

Stress intensity factor for three point bend (single edged notch) specimen is [30,37,38],

$$K_{Srawley} = \frac{3(S/W)\left(P/B\sqrt{W}\right)\sqrt{\alpha}\;\left[1.99 - \alpha(1-\alpha)(2.15 - 3.93\,\alpha + 2.7\,\alpha^2)\right]}{2\,(1+2\alpha)(1-\alpha)^{3/2}} \tag{12}$$

Stress intensity factor for three point bend (single edged notch) specimen by Tada et al. [39], is,

$$K_{Tada} = \sigma \sqrt{\pi a}\ F(\alpha) \tag{13}$$

$$\sigma = \frac{6M}{W^2} \tag{14}$$

$$M = \frac{PS}{4} \tag{15}$$

$$F(\alpha) = \frac{1}{\sqrt{\pi}} \cdot \frac{1.99 - \alpha(1-\alpha)(2.15 - 3.93\,\alpha + 2.7\,\alpha^2)}{(1+2\,\alpha)(1-\alpha)^{3/2}} \tag{16}$$

By substituting equations (14)–(16) into equation (13) gives,

$$K_{Tada} = \frac{3(S/W)\left(P/\sqrt{W}\right)\sqrt{\alpha}\left[1.99 - \alpha(1-\alpha)(2.15 - 3.93\alpha + 2.7\alpha^2)\right]}{2(1+2\alpha)(1-\alpha)^{3/2}} \tag{17}$$

Where, S = Support span; P = Applied load; B = Thickness; W = Depth; $\alpha = a/W$; a = average crack length; M = Applied moment and σ = Bending stress.

From equations (12) and (17), can be noted that,

$$K_{Tada} = B\ K_{Srawley} \tag{18}$$

Srawley [30] considered the thickness to derive the SIF whereas Tada et al. [39], is not defined. SIF computed using Srawley [30] is directly proportional to SIF computed using Tada et al. [39], wherein thickness is constant of proportionality.

3. Numerical analysis

Single edge notched bend (SENB) specimen made up of ferritic steel (SA 508 Gr.3 Cl.1), austenitic steel (SA312 Type 304LN) and Inconel – 182 alloy (ENiCrFe-3) under three point bending has been studied by using 2-D and 3-D FEA. The length (L), depth (W) and thickness (B) is 148 mm, 32 mm and 16 mm respectively. The geometrical configuration is detailed in Table 1 and shown in Fig. 2. 2-D FEA has been carried for unit and 16 mm thickness. 3-D FEA is carried out for 16 mm thickness. The geometrical configuration is taken from Wang et al., [6]. The crack is located at the center of the specimen and the crack lengths are 0.5W, 0.625W and 0.75W. Material properties are given in Table 2 [40]. 2-D and 3D FEAs of homogenous [ferritic steel/austenitic steel/Inconel – 182 alloy (Weld)] have been performed to validate with the analytical solutions.

2-D four noded plane strain element and 3-D eight noded solid elements are employed for the modeling. Reduced integration with full newton raphson method is employed in the numerical procedure to solve the 2-D and 3-D problem. Load is taken as 1 kN for the analysis purpose. Fracture analysis is carried out for the predicted crack growth. Contour integral method and XFEM are employed to extract the SIF in 2-D and 3-D respectively. Maximum tangential stress criterion is used to extract the SIF around the crack tip which was proposed by Matvienko [41]. FEA is conducted for several combinations by using the data tabulated in Tables 1 and 2. 2-D and 3-D FEA of homongeous SENB made up of Ferritic or Austenitic or Weld under three poing bending for different crack configurations as discussed earlier is carried out to validate the available analytical solutions.

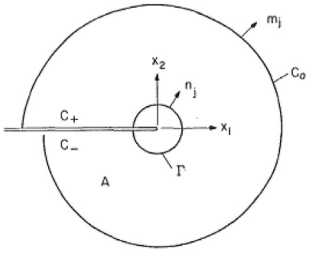

Fig. 1. J-integral domain A enclosed by Γ.

Table 1
Geometry and crack configuration.

Crack length, (mm)		D (mm)						t (mm)	
								2D	3D
16	H	5	10	20	30	40	50	Unit	–
20	H	5	10	20	30	40	50		
24	H	5	10	20	30	40	50		
16	H	5	10	20	30	40	50	16	16
20	H	5	10	20	30	40	50		
24	H	5	10	20	30	40	50		

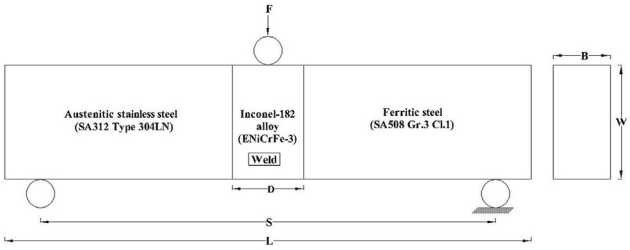

Fig. 2. Geometrical configuration of SENB.

Table 2
Material properties.

Material	Young's modulus, GPa	μ
SA 508 Gr.3 Cl.1 (Ferritic)	227	0.3
SA312 Type 304LN (Austenitic)	184	0.3
ENiCrFe-3 (Weld/Inconel – 182 alloy)	192	0.3

4. Results and discussions

4.1. 2-D FEA of dissimilar metal SENB

Analytical SIF is obtained by eqn (12) and eqn (17) for 16 mm thickness and unit thickness respectively for all crack configurations detailed in Table 1 and for the crack configurations [Ferritic/Austenitic/Weld] SIF is computed by numerically (2-D and 3-D FEA). SIF vs crack length with respect to the DMJW is shown in Fig. 3 for 16 mm thickness and is found that, eqn (18) is valid. The analytical SIF for the crack lengths of 16 mm, 20 mm and 24 mm is 3.72, 5.825 and 10.771 MPa$\sqrt{m}$ respectively. 2-D FEA resulted that, SIF of homogenous material for the crack length of 16 mm, 20 mm and 24 mm is 2.921, 4.892 and 10.015 respectively. The percentage difference between the analytical and 2-D FEA (Fig. 5) for the crack lengths of 16 mm, 20 mm and 24 mm is 21.5%, 15.99% and 7.02% respectively. Predicted SIF values with respect to the thickness effect is expressed by eqn (18). Fracture behavior of the coolant piping component is dependence on loading rate for ferritic steel wherein the stainless steel is independent [22]. Out-of-plane

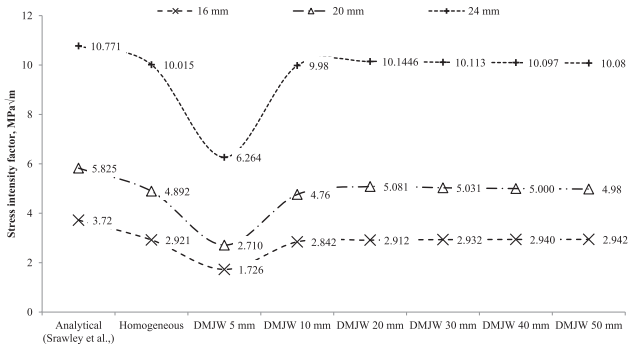

Fig. 3. Crack length vs SIF for various DMJW (16 mm thickness, P = 1 kN).

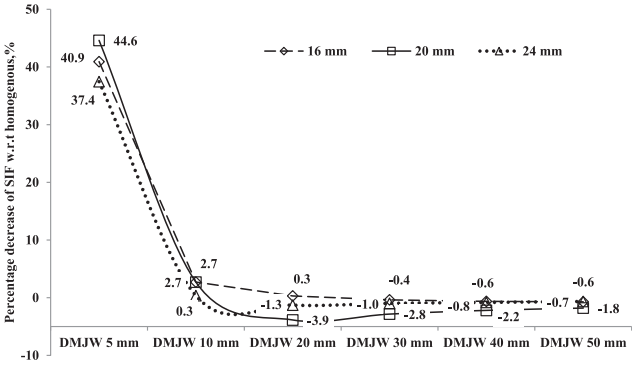

Fig. 4. Percentage decrease of SIF for various crack lengths of DMJW w.r.t homogenous.

constraint effects (thickness effect) resulted that the decrease in fracture resistance with increase of thickness due to the existence of plane strain condition [23]. The percentage decrease of SIF with respect to homongeous is found to be similar with respect to varying thickness; and a typical plot is shown in Fig. 4. The increase or decrease of fracture toughness is dependent on the out-of-plane constraint [28].

For DMJW 5 mm, SIF is 1.726, 2.710 and 6.264 MPa$\sqrt{m}$ for the crack lengths of 16 mm, 20 mm and 24 mm respectively. For the case of DMJW 5 mm, the percentage reduction of SIF for the crack lengths of 16 mm, 20 mm and 24 mm is 40.9%, 44.6% and 37.4% compared to homogenous respectively. Further, it is observed that the SIF is found to be significantly less for the case of DMJS of 5 mm compared to homogenous. The reason could be material mismatch at larger scale. The maximum percentage decrease of SIF with respect to homogenous for DMJW of 10 mm, 20 mm, 30 mm, 40 mm and 50 mm is up to 2.7% (0.3% to 2.7%), −3.9% (0.3% to −3.9%), −2.8% (−0.4% to −2.8%), −2.2% (−0.4% to −2.2%) and −1.8% (−0.6 to −1.8%) respectively for all crack lengths. From Fig. 4, it can be observed that, the percentage decrease of SIF with respect to homogenous is in between −3.9% and 2.7% for all DMJWs expect for 5 mm which is due to the constraing effect of material mismatch.

The stress distribution for homogenous is found to be similar for both unit and 16 mm thickness. A typical stress distribution contour is given in Fig. 5. Stress contours around the crack tip increases gradually with respect to the DMJWs and can be seen by closer examination of Fig. 5. The effect of DMJW can be seem significant for DMJW 5 mm and 10 mm (Fig. 4). For the homogenous case from Fig. 5, it can be observed that, the near symmetrical stress distribution is exhibited due to the support constraints and area of yield zone decreases with increase of crack length. From Fig. 5, it can be observed that, the interface of austenitic zone starts to yield due to the material heterogenity and is exhibited clearly for a/W = 0.5 for DMJW of 5 mm and 10 mm. Since, the DMJ zone yields first and the stresses are distributed towards the austenitic and ferritic zones through the interfaces in which the ferritic interface exhibiting

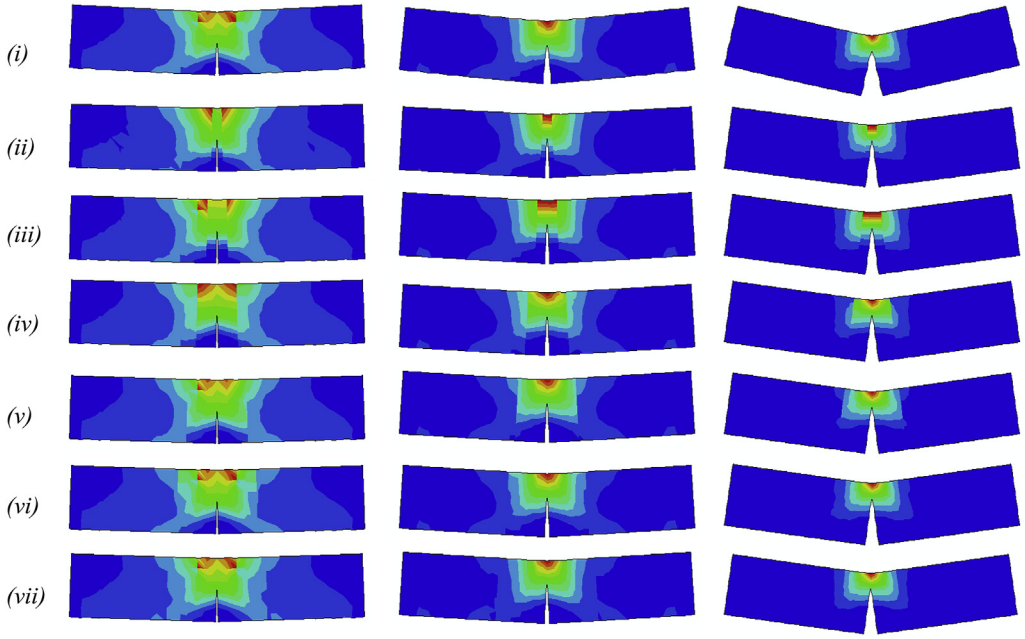

(i) Homogenous; *(ii) DMJW of 5 mm; (iii) DMJW of 10 mm; (iv) DMJW of 20 mm; (v) DMJW of 30 mm; (vi) DMJW of 40 mm; (vii) DMJW of 50 mm*

Fig. 5. Stress distribution of 2-D SENB.

little high stress distribution than austenitic even the near support is roller due to the strength mismatch. However, the DMJs exhibits less stress distribution level than the austenitic and ferritic due tranfer mechanism even though the strength of the DMJ is less than ferritic. From Fig. 5, it can be summarized that, the geometrical and material constraints plays a major role in the stress distribution and the constraint effects of geometry have been clearly observed for DMJWs of 5 mm and 10 mm. Significant stress transfer mechanism is observed for DMJW of 5 mm and 10 mm.

For the DMJWs except 5 mm and 10 mm, exhibiting the similar effects on geometrical constraint and material mismatch with different stress distribution and is seen in Fig. 5. Austenitic-DMJ interface seems be high yield zone than ferritic-DMJ due to the inhomogeneity wherein the stress transfer mechanism occurs locally in the DMJs, observed for DMJW of 20 mm, 30 mm, 40 mm and 50 mm. For DMJW of 20 mm, stress level is very high in the interfaces than larger DMJWs due to the geometrical constraint effect with respect to the specimen size. Near symmetrical stress distribution is observed for the DMJWs of 20 mm, 30 mm, 40 mm and 50 mm whereas the yield zone of the different stress contour is quite high in austenitic region with respect to the strength mismatch.

4.2. 3-D FEA of dissimilar metal SENB

3-D simulations have been performed for the configurations detailed in Table 1 and Fig. 2. 3-D FEA is conducted for 16 mm thickness to understand the fracture behavior of the specimen. Effect of thickness is considered in eqn (12) and the same is validated with the 3-D FEA. Element size of 2 mm is considered through mesh sensitivity analysis. SIF obtained for homogenous made up of Ferritic or Austenitic or Weld through 3-D FEA for crack lengths of 16 mm, 20 mm and 24 mm is 4.241, 6.214 and 9.784 MPa$\sqrt{m}$ respectively. The percentage difference between the analytical and 3-D FEA is −13.97%, −6.76% and 9.20% for the crack lengths of 16 mm, 20 mm and 24 mm respectively. Also, it can be noted that the percentage difference of SIF is in between −14% and 9% for all crack lengths clearly stating that, the analytical solution can be compromised within ±15% with respect to 3-D FEA for the structural integrity analysis of structures/components using LEFM principles. FE computation in the 3-D analysis can offer more conservative results than the analytical wherein the analytical was arrived at based on the boundary collocation method. Crack length vs SIF with respect to DMJW is shown in Fig. 6, wherein the applied load is 1 kN.

The percentage decrease of SIF with respect to homogenous is plotted in Fig. 7. For a particular crack length of 16 mm, the percentage decrease of SIF with respect to homogenous is 6.3%, 2.8%, 1.6%, 0.8% and 0.6% for the DMJW of 5 mm, 10 mm, 20 mm, 30 mm

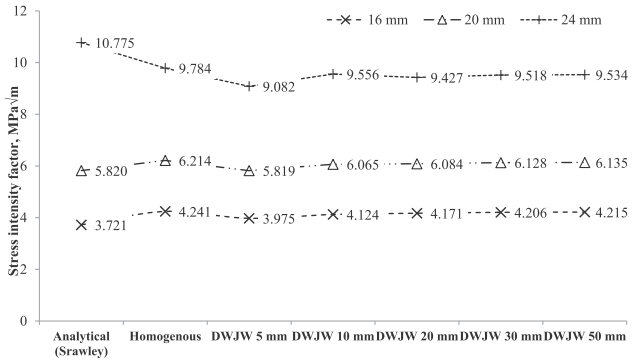

Fig. 6. Crack length vs SIF for various DMJW (P = 1 kN).

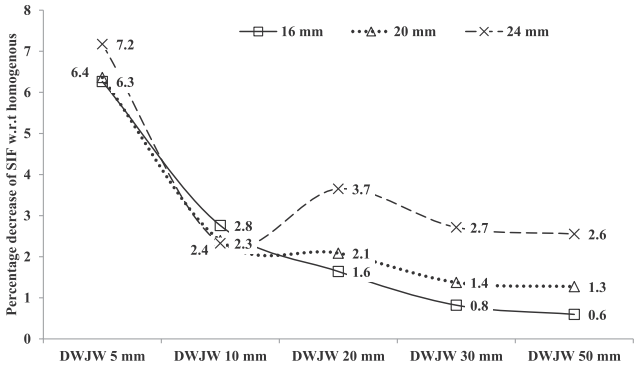

Fig. 7. Percentage decrease of SIF w.r.t homogenous for various crack lengths.

and 50 mm respectively. For all crack lengths, the percentage decrease of SIF with respect to the homogenous is within 4% for all DMJWs except DMJW of 5 mm and is shown in Fig. 7. For DMJW of 30 mm and 50 mm, the percentage decrease of SIF with respect to homogenous is found to be similar for all crack lengths. The percentage decrease of SIF with respect to homogenous for DMJW of 10 mm is found to be similar for all crack lengths except 16 mm for which 0.4% increase is observed. The percentage decrease of SIF with respect to homogenous for DMJW of 5 mm is found to be similar for all crack lengths except 24 mm, for which 0.8% increase is observed. For all the cases SIF found to increase with crack length. For DMJW of 20 mm, percentage decrease of SIF with respect to homogenous is 1.6%, 2.1% and 3.7% for the crack lengths of 16 mm, 20 mm and 24 mm respectively. The percentage difference of SIF beyond DMJW 20 mm is near similar and hence can be suggested as optimal configuration for DMJs.

3-D stress distribution for several DMJWs is shown in Fig. 8. For homogeneous case, influence of yield zone around crack tip is large for smaller discontinuities which lead to higher requirement of energy dissipation than larger discontinuities. By closer examination, the dissimilar metal SENB exhibiting high stress at the interfaces of the material discontinuity. For the smaller crack length, the size of yield zone contours increased with increase of DMJWs due to the material mismatch and is found to be significant effect for DMJW of 5 mm and 10 mm due to the excessive constrain at the interfaces. For the case of homogenous from Fig. 8 (i), the increase of contour on yield zone is observed for near roller support. The stress around the crack tip starts towards the DMJ-ferritic interface and extends in opposite nature towards the DMJ-austenitic interface, since the material mismatch occurs in the joint for the case of DMJWs except 5 mm and 10 mm. 3-D stress distribution of DMJWs with respect to the crack length is found to be linear and the geometrical constraint dominance is less significance than 2-D for DMJW of 5 mm and 10 mm. However, the near stress distribution is exhibited due to the pronounced material mismatch effect. The simulated results of 3-D stress distribution leads to realistic behavior, since the crack tip constraint effect is observed whereas the 2-D FEA does not exhibits the crack tip constraint effect.

The distribution of stress over the specimen plays the major role in the life components. SIF has to concern with the presence of stress distribution. Computed SIF is found around the crack tip and the stress distribution exhibiting the material mismatch over the specimen with reference to the homogenous. Hence, the understanding of the stress distribution around the crack is also a significance to study the behavior of the specimen.

5. Summary

Numerical investigations on DMSENB specimens subjected to

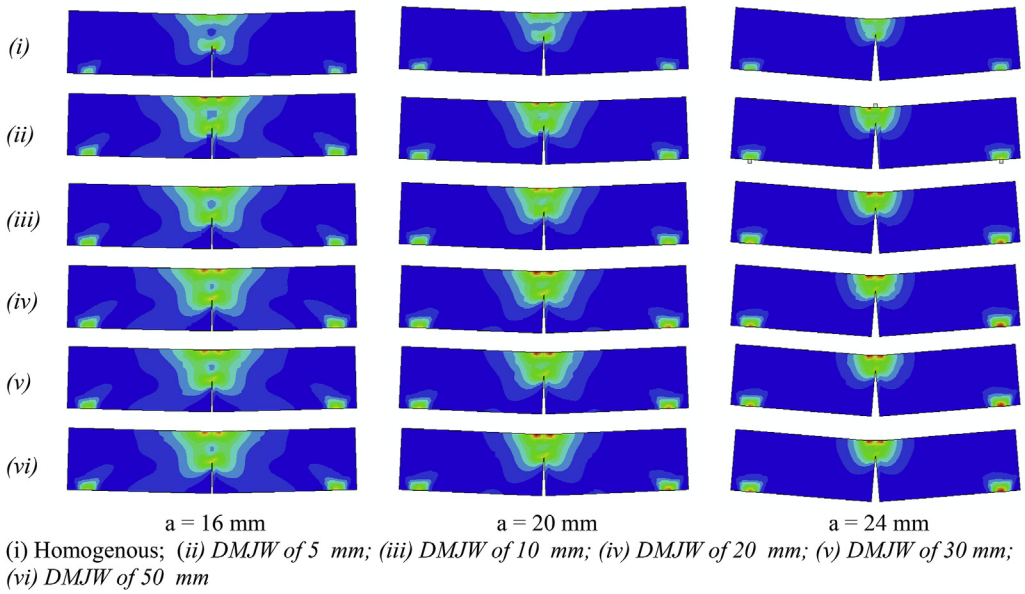

(i) Homogenous; *(ii) DMJW of 5 mm; (iii) DMJW of 10 mm; (iv) DMJW of 20 mm; (v) DMJW of 30 mm; (vi) DMJW of 50 mm*

Fig. 8. Stress distribution of 3-D SENB.

three point bending is carried out to study the fracture behavior of DMJs. DMSENB specimens comprise of ferritic steel, austenitic steel and Inconel – 182 alloy. Crack growth studies are performed in 2-D and 3-D FEA to evaluate the SIF using LEFM principles. Contour integral method and XFEM is employed in the fracture study for 2-D and 3-D FEA respectively. A bench mark study is done on homogenous SENB specimen made up of ferritic steel or austenitic steel or Inconel – 182 alloy to validate with the available analytical solution and the results exhibit a good agreement. Fracture studies are performed on DMSENB specimens with (i) DMJW (geometrical constraints) (ii) strength mismatch (material constraints) (iii) thickness and (iv) crack lengths to study the DMJ behavior. 2-D FEA of DMSENB specimen resulted that, SIF is linear with respect to the thickness. The stress distribution is found to be similar with respect to the thickness. Geometrical constraint effect is observed for DMJW of 5 mm in 2-D FEA. The constraint effect of DMJW of 5 mm and 10 mm has been observed by closer examination of stress distribution in 2-D FEA of DMSENB specimen and the results are related to the strength mismatch effects. Local stress transfer mechanism is observed in the DMJs for all DMJWs except 5 mm and 10 mm due to the material heterogeneity and the effect of geometrical constraints wherein the strength mismatch is identified at the interface of the materials from the stress distribution. Studies carried out on 3-D FEA of homogenous SENB specimens show that, the computed SIF is higher than analytical for a/W ratios of 0.5 and 0.625; and is less than analytical [30] for a/W of 0.75 due to the mesh sensitivity with respect to the crack configuration. Computed SIF using 3-D FEA is significantly larger than 2-D analytical solution [30] with maximum difference of 15%. 3-D FEA of DMSENB specimens show that, SIF increases with DMJW for all respective crack lengths except DMJW of 10 mm for a/W of 0.75. Based on the several parametric studies, it has been observed that the difference in SIF for particular crack length beyond DMJW of 20 mm is not significant i.e., the constraint effect due to the strength mismatch and DMJWs are insensitive for the evaluation of the fracture parameter. The constraint effect is found to be significant if DMJW is less than 20 mm and the ratio of specimen length to the DMJW is greater than 7.4. 3-D stress distribution results, the larger discontinuities can be fractured with minimum requirement of energy dissipation. Yield zone size increases with DMJWs for smaller discontinuities due to the material mismatch effect and the pronounced effect of excessive constraint is observed at the interfaces for DMJW of 5 mm and 10 mm. Effect of geometrical constraint is less significance in 3-D FEA leads to realistic analysis. Crack tip constraint effect can be clearly observed from the 3-D FEA rather than 2-D FEA and is in reliable manner to exhibit the realistic behavior.

In general, SIF represents the strength of crack in the vicinity of the crack tip. It is an important fracture parameter to predict the remaining life and residual strength of the structure/components. The predicted life or residual strength will in turn useful to take decisions for maintenance schedule, repair and retrofitting of the structures/components of nuclear industry or other related industries.

Declaration of competing interest

We would like to state that there is no conflict of interest on manuscript entitled, “Effect of dissimilar metal SENB specimen width and crack length on stress intensity factor” authored by A. Ramachandra Murthy, Muthu Kumaran M, M. Saravanan, P. Gandhi for possible publication in Nuclear Engineering and Technology.

References

[1] Bin Qiang, Xin Wang, Ductile crack growth behaviors at different locations of a weld joint for an X80 pipeline steel: a numerical investigation using GTN models, Eng. Fract. Mech. 213 (2019) 264–279, https://doi.org/10.1016/j.engfracmech.2019.04.009.

[2] M.K. Samal, M. Seidenfuss, E. Roos, K. Balani, Investigation of failure behavior of ferritic-austenitic type of dissimilar steel welded joints, Eng. Fail. Anal. 18 (2011) 999–1008, https://doi.org/10.1016/j.engfailanal.2010.12.011.

[3] H.T. Wang, G.Z. Wang, F.Z. Xuan, S.T. Tu, An experimental investigation of local fracture resistance and crack growth paths in a dissimilar metal welded joint, Mater. Des. 44 (2013) 179–189, https://doi.org/10.1016/j.matdes.2012.07.067.

[4] Sachin Kumar, I.V. Singh, B.K. Mishra, XFEM simulation of stable crack growth using J-R curve under finite strain plasticity, Int. J. Mech. Mater. Des. 10 (2014) 165–177, https://doi.org/10.1007/s10999-014-9238-1.

[5] Haitao Wang, Guozhen Wang, Fuzhen Xuan, Changjun Liu, Shantung Tu, Local mechanical properties and microstructures of Alloy52M dissimilar metal welded joint between A508 ferritic steel and 316L stainless steel, Adv. Mater.

Res. 509 (2012) 103–110, https://doi.org/10.4028/www.scientific.net/AMR.509.103.
[6] H.T. Wang, G.Z. Wang, F.Z. Xuan, S.T. Tu, Numerical investigation of ductile crack growth behavior in a dissimilar metal welded joint, Nucl. Eng. Des. 241 (2011) 3234–3243, https://doi.org/10.1016/j.nucengdes.2011.05.010.
[7] B. Younise, M. Rakin, N. Gubeljak, B. Medjob, A. Sedmak, Effect of material heterogeneity and constraint conditions on ductile fracture resistance of welded joint zones – micromechanical assessment, Eng. Fail. Anal. 82 (2017) 435–445, https://doi.org/10.1016/j.engfailanal.2017.08.006.
[8] K. Karthick, S. Malarvizhi, V. Balasubramanian, S.A. Krishnan, G. Sasikala, Shaju K. Albert, Tensile and impact toughness properties of various regions of dissimilar joints of nuclear grade steels, Nucl. Eng. Technol. 50 (2018) 116–125, https://doi.org/10.1016/j.net.2017.10.003.
[9] Primož Štefanea, Sameera Naib, Stijn Hertelé, Wim De Waele, Nenad Gubeljak, Crack tip constraint analysis in welded joints with pronounced strength and toughness heterogeneity, Theor. Appl. Fract. Mech. 103 (2019) 102293, https://doi.org/10.1016/j.tafmec.2019.102293.
[10] K. Fan, G.Z. Wang, F.Z. Xuan, S.T. Tu, Local fracture resistance behavior of interface regions in a dissimilar metal welded joint, Eng. Fract. Mech. 136 (2015) 279–291, https://doi.org/10.1016/j.engfracmech.2015.02.007.
[11] Ad Bakker, Elastic-plastic fracture mechanics analysis of an SENB specimen, Int. J. Press. Vessel. Pip. 10 (1982), https://doi.org/10.1016/0308-0161(82)90004-7. .
[12] J. Xu, Z.L. Zhang, E. Østby, B. Nyhus, D.B. Sun, Effects of crack depth and specimen size on ductile crack growth of SENT and SENB specimens for fracture mechanics evaluation of pipeline steels, Int. J. Press. Vessel. Pip. 86 (2009) 787–797, https://doi.org/10.1016/j.ijpvp.2009.12.004.
[13] J. Yang, G.Z. Wang, F.Z. Xuan, S.T. Tu, Unified characterisation of in-plane and out-of-plane constraint based on crack-tip equivalent plastic strain, Fatigue Fract. Eng. M. 36 (2012) 504–514, https://doi.org/10.1111/ffe.12019.
[14] J. Wang, G.Z. Wang, F.Z. Xuan, S.T. Tu, Derivation of constraint-dependent J-R curves based on modified T-stress parameter and GTN model for a low alloy steel, Int. J. Fract. 183 (2013) 155–168, https://doi.org/10.1007/s10704-013-9884-6.
[15] J. Yang, G.Z. Wang, F.Z. Xuan, S.T. Tu, C.J. Liu, An experimental investigation of in-plane constraint effect on local fracture resistance of a dissimilar metal welded joint, Mater. Des. 53 (2014) 611–619, https://doi.org/10.1016/j.matdes.2013.07.058.
[16] J. Yang, G.Z. Wang, F.Z. Xuan, S.T. Tu, Unified correlation of in-plane and out-of-plane constraint with fracture resistance of a dissimilar metal welded joint, Eng. Fract. Mech. 115 (2014) 296–307, https://doi.org/10.1016/j.engfracmech.2013.11.018.
[17] C.A. Della Rovere, C.R. Ribeiro, R. Silva, N.G. Alcântara, S.E. Kuri, Local mechanical properties of radial friction welded supermartensitic stainless steel pipes, Mater. Des. 56 (2014) 423–427, https://doi.org/10.1016/j.matdes.2013.11.020.
[18] Marco Gonzalez, Paulo Teixeira, Jeanette Gonzalez, Raul Machado, Numerical analysis of fracture mechanics of SENB specimens prepared from HDPE pipes, in: Proceedings of the ASME 2014 Pressure Vessels & Piping Conference, California, USA, 2014, https://doi.org/10.1115/PVP2014-28718. July 20-24.
[19] M.Y. Mu, G.Z. Wang, F.Z. Xuan, S.T. Tu, Unified correlation of in-plane and out-of-plane constraints with cleavage fracture toughness, Theor. Appl. Fract. Mech. 80 (2015) 121–132, https://doi.org/10.1016/j.tafmec.2015.10.005.
[20] K. Fan, G.Z. Wang, F.Z. Xuan, S.T. Tu, Local failure behavior of a dissimilar metal interface region with mechanical heterogeneity, Eng. Fail. Anal. 59 (2016) 419–433, https://doi.org/10.1016/j.engfailanal.2015.11.005.
[21] Jin Weon Kim, Myung Rak Choi, Yun Jae Kim, Effect of loading rate on the fracture behavior of nuclear piping materials under cyclic loading conditions, Nucl. Eng. Technol. 48 (2016) 1376–1386, https://doi.org/10.1016/j.net.2016.06.006.
[22] W. Musraty, B. Medjo, N. Gubeljak, A. Likeb, I. Cvijović-Alagić, A. Sedmak, M. Rakin, Ductile fracture of pipe-ring notched bend specimens - micromechanical analysis, Eng. Fract. Mech. 175 (2017) 247–261, https://doi.org/10.1016/j.engfracmech.2017.01.022.
[23] Jie Yang, Lei Wang, Fracture mechanism of cracks in the weakest location of dissimilar metal welded joint under the interaction effect of in-plane and out-of-plane constraints, Eng. Fract. Mech. 192 (2018) 12–23, https://doi.org/10.1016/j.engfracmech.2018.02.008.
[24] Jiankai Tang, Liu Zheng, Shouwen Shi, Xu Chen, Evaluation of fracture toughness in different regions of weld joints using unloading compliance and normalization method, Eng. Fract. Mech. 195 (2018) 1–12, https://doi.org/10.1016/j.engfracmech.2018.03.022.
[25] Dai Yue, Jie Yang, Lei Wang, Effect range of the material constraint-II, Interface crack, Metals 9 (1–10) (2019) 696, https://doi.org/10.3390/met9060696.
[26] B. Vieille, J.D. Pujols Gonzalez, C. Bouvet, Prediction of the ultimate strength of quasi-isotropic TP-based laminates from tensile and compressive fracture toughness at high temperature, Compos. B Eng. 164 (2019) 437–446, https://doi.org/10.1016/j.compositesb.2019.01.056.
[27] Jian-Ping Zuo, Yu-Lin Li, Cunhui Liu, Hai-yan Liu, Jintao Wang, Hong-tao Li, Lei Liu, Meso-fracture mechanism and its fracture toughness analysis of Longmaxi shale including different angles by means of M-SENB tests, Eng. Fract. Mech. 215 (2019) 178–192, https://doi.org/10.1016/j.engfracmech.2019.05.009.
[28] Junnan Lv, Li Yu, Wei Du, Qun Li, Theoretical approach of characterizing the crack-tip constraint effects associated with material's fracture toughness, Arch. Appl. Mech. 88 (2018) 1637–1656, https://doi.org/10.1007/s00419-018-1392-8.
[29] J. Wang, G.Z. Wang, F.Z. Xuan, S.T. Tu, Constraint-Dependent J-R curves of a dissimilar metal welded joint for connecting pipe-nozzle of nuclear pressure vessel, J. Press. Vessel Technol. 137 (1–8) (2014), 021405, https://doi.org/10.1115/1.4028993.
[30] E. John, Srawley, Wide range stress intensity factor expressions for ASTM E 399 standard fracture toughness specimen, Int. J. Fract. 12 (1976) 475–476, https://doi.org/10.1007/BF00032844.
[31] B. Moran, C.F. Shih, Crack tip and associated domain integrals from momentum and energy balance, Eng. Fract. Mech. 27 (1987) 615–642, https://doi.org/10.1016/0013-7944(87)90155-X.
[32] C.F. Shih, R.J. Asaro, Elastic-plastic analysis of cracks on bimaterial interfaces: Part I - small scale yielding, J. Appl. Mech. 55 (1988) 299–316, https://doi.org/10.1115/1.3173676.
[33] Osher Stanley, James A. Sethian, Fronts propagating with curvature-dependent speed: algorithms based on Hamilton-Jacobi formulations, J. Comput. Phys. 79 (1988) 12–49, https://doi.org/10.1016/0021-9991(88)90002-2.
[34] M. Stolarska, D.L. Chopp, N. Moes, T. Belytschko, Modelling crack growth by level sets in the extended finite element method, Int. J. Numer. Methods Eng. 51 (2001) 943–960, https://doi.org/10.1002/nme.201.
[35] N. Sukumar, D.L. Chopp, B. Moran, Extended finite element method and fast marching method for three-dimensional fatigue crack propagation, Eng. Fract. Mech. 70 (2003) 29–48, https://doi.org/10.1016/S0013-7944(02)00032-2.
[36] T. Belytschko, T. Black, Elastic crack growth in finite elements with minimal remeshing, Int. J. Numer. Methods Eng. 45 (1999) 601–620, https://doi.org/10.1002/(SICI)1097-0207(19990620)45:5%3C601::AID-NME598%3E3.0.CO;2-S.
[37] ASTM E1820-01, Standard Test Method for Measurement of Fracture Toughness, ASTM International, US, 2001. www.astm.org.
[38] ASTM E399-17, Standard Test Method for :Linear-Elastic Plane Strain Fracture Toughness KI_C of Metallic Materials, ASTM International, US, 2018. www.astm.org.
[39] Hiroshi Tada, Paul C. Paris, George R. Irwin, The Stress Analysis of Cracks Handbook, third ed., ASME Press, 2000 https://doi.org/10.1115/1.801535.
[40] S. Kumar, P.K. Singh, K.N. Karn, V. Bhasin, Experimental investigation of local tensile and fracture resistance behavior of dissimilar metal weld joint: SA508 Gr.3 Cl.1 and SA312 Type 304LN, Fatigue Fract. Eng. M. 40 (2016) 190–206, https://doi.org/10.1111/ffe.12484.
[41] Yu G. Matvienko, Maximum average tangentical stress criterion for prediction of the crack path, Int. J. Fract. 176 (2012) 113–118, https://doi.org/10.1007/s10704-012-9715-1.